FULL PAPER

Magnetic Control of Tubular Catalytic Microbots for the Transport, Assembly, and Delivery of Micro-objects

By *Alexander A. Solovev, Samuel Sanchez,* Martin Pumera, Yong Feng Mei,** and *Oliver G. Schmidt*

Recently a significant amount of attention has been paid towards the development of man-made synthetic catalytic micro- and nanomotors that can mimic biological counterparts in terms of propulsion power, motion control, and speed. However, only a few applications of such self-propelled vehicles have been described. Here the magnetic control of self-propelled catalytic Ti/Fe/Pt rolled-up microtubes (microbots) that can be used to perform various tasks such as the selective loading, transportation, and delivery of microscale objects in a fluid is shown; for instance, it is demonstrated for polystyrene particles and thin metallic films ("nanoplates"). Microbots self-propel by ejecting microbubbles via a platinum catalytic decomposition of hydrogen peroxide into oxygen and water. The fuel and surfactant concentrations are optimized obtaining a maximum speed of 275 μm s^{-1} (5.5 body lengths per second) at 15% of peroxide fuel. The microbots exert a force of around 3.77 pN when transporting a single 5 μm diameter particle; evidencing a high propulsion power that allows for the transport of up to 60 microparticles. By the introduction of an Fe thin film into the rolled-up microtubes, their motion can be fully controlled by an external magnetic field.

1. Introduction

The control over micro- and nanoobjects has attracted great attention in several areas of science, such as nanotechnology and drug delivery. One of the major challenges is to achieve autonomous movement of micro- and nanoscale machines in a fluid and employ them to perform complex tasks such as drug delivery, transport, and assembly of micro-/nano-objects.[1]

[*] Dr. S. Sanchez, Dr. Y. F. Mei, A. A. Solovev, Prof. O. G. Schmidt
Institute for Integrative Nanosciences, IFW Dresden
Helmholtzstrasse 20, D-01069 Dresden, 01069 (Germany)
E-mail: s.sanchez@ifw-dresden.de; y.mei@ifw-dresden.de
Dr. S. Sanchez
WPI-MANA, National Institute for Materials Science
Tsukuba, Ibaraki, 305-0044 (Japan)
Dr. M. Pumera
Biomaterials Center, National Institute for Materials Science
Tsukuba, Ibaraki, 305-0044 (Japan)
Dr. M. Pumera
Division of Chemistry and Biological Chemistry, School of Physical & Mathematical
Sciences, Nanyang Technological University 637371 (Singapore)

Richard Feynman in his 1959 speech "There's Plenty of Room at the Bottom" envisioned microscopic factories with tiny machines that could perform sophisticated tasks.[2] The dream of manufacturing nanomachines is to mimic biological motors that can convert chemical into mechanical energy and hence develop diverse functions.[3] Some fascinating examples in nature are DNA and RNA polymerase;[4] rotary motors such as ATP synthase;[5] cilia and flagella motors;[6] dyneins,[7] kinesins,[8] and myosins.[9]

Catalytic synthetic micro- and nanomotors[10–13] and engines[14,15] are of growing interest because of their high locomotive power and easy control.[16] Several approaches have been focused on the improvement of the catalytic conversion of chemicals (e.g., hydrogen peroxide) into kinetic energy[17–19] and the control over the movement of nanomotors by different sources has been reported.[20]

The transport of spherical particles used as cargo[21,22] was recently achieved by either using electrostatic, chemical, or magnetic interactions to attach the cargo.[21,22] Extra functionality has also been given to the cargo (e.g., magnetic properties, chemical modification for electrostatic binding) for loading into the nanomotors. In addition, practical applications require higher towing forces and general mechanisms to bind and unbind different cargo in an easy and controllable way. Recently, rolled-up tubular structures that accumulate gas, which is generated by the catalytic decomposition of a fuel, have been developed.[14] These tubular microjets enhance the power of synthetic micromachines reaching a speed of up to 50 body lengths per second.[15]

In this work, we describe the use of rolled-up thin Ti/Fe/Pt films as microbots developing tasks that require full control over their motion and high propulsion power. Maneuvers of self-propelled microbots were wirelessly coordinated by an external magnetic field, which allows the selective manipulation of different micro-objects randomly suspended in solution. The physical characteristics of these tubular microbots led to a high propulsion power and allowed more than sixty polymeric cargo-particles to be attached and transferred to a desired location. Moreover, we achieved the selective loading of metallic nanoplates with a "large" surface area, their transport and directed assembly into different configurations. These illustrative examples form an attractive concept of

wireless transport and ''bottom-up'' assembly of various materials from discrete building blocks, which is so familiar and widespread in natural systems.

2. Results and Discussion

2.1. Microfactory

The tubular microbots were synthesized from thin films according to previously published procedures using ''rolled-up'' nanotechnology.[14,23] We successfully rolled-up metallic Ti/Fe/Pt thin films into microtubes ($5.0 \pm 0.4\,\mu m$ in diameter and $50\,\mu m$ in length) by selective under-etching of polymer sacrificial patterns and controlling the deposition thickness, angle, and rates.[14] Figure 1A shows a schematic diagram of an array of rolled-up microtubes integrated on a planar silicon substrate fabricated using photolithography, deposition, and undercutting. The microtubes started to work as valve-less catalytic pumps once hydrogen peroxide was added as chemical fuel. The catalytic decomposition of the peroxide generated microbubbles in the tubular cavities[14,24] and induced a mechanical force (i.e., pumping of fluid) through the tubes. Video #1 in the Supporting Information shows details of the catalytic pumping of these tubes integrated on a silicon substrate. The direction of bubble migration is defined strongly by the fluid flow resistance, which is significantly higher for smaller tubular openings. Indeed, the small difference in the opening sizes of the tubes causes the bubbles to migrate and eject from the larger tubular opening, as has been explained previously.[15] Similar effects are observed for blood circulation in vessels where a very small change in diameter leads to large changes in the flow resistance.[25]

Figure 1B depicts the different moving trajectories of self-propelled microbots in the fuel solution after being released from the substrate. The microtubes could be released from the substrate: i) by means of gentle mechanical scratching or ii) by oxygen bubbles that are continuously generated whereby the buoyancy force lifts the microtubes up to the liquid–gas interface. The different trajectories of our microbots can be explained by the asymmetry in the rolled-up layers consequently leading to an asymmetric release of the bubbles and inhomogeneous fluid flow through and around the tube. The motions of our self-propelled synthetic microbots can be divided into straight, circular, and three-dimensional helical trajectories.[15] Such autonomous motions are like those of bacteria, suggesting that physical parameters such as the distribution of torque around tubular bodies are similar for both synthetic and biological moving objects.[26] The evolution of torque was described in detail for *Listeria monocytogenes*, pathogens that self-propel by asymmetric actin growth.[27] Fascinating examples of bacteria engines are cells that use a gliding motility based on nanoscale nozzle-like structures. *Myxococcus xanthus* is an example of this type of motility with nanojets working by expelling polyelectrolyte slime from several hundreds of nanonozzles.[28] Although our synthetic microbot contains only one nozzle, which is two orders of magnitude larger in comparison to *M. xanthus*, its speed is up to two hundred times faster than that of the bacteria.

As ferromagnetic (Fe) layers were integrated into the tubular walls, the motion of the microbots could easily be directed and wirelessly controlled by positioning a mechanical actuator containing a permanent magnet, as depicted in Figure 1C. An external small NdFeB magnet ($10\,mm \times 7\,mm \times 5\,mm$), producing a field of 50 G around the samples, was placed underneath a suspension of the microbots at a distance close enough to
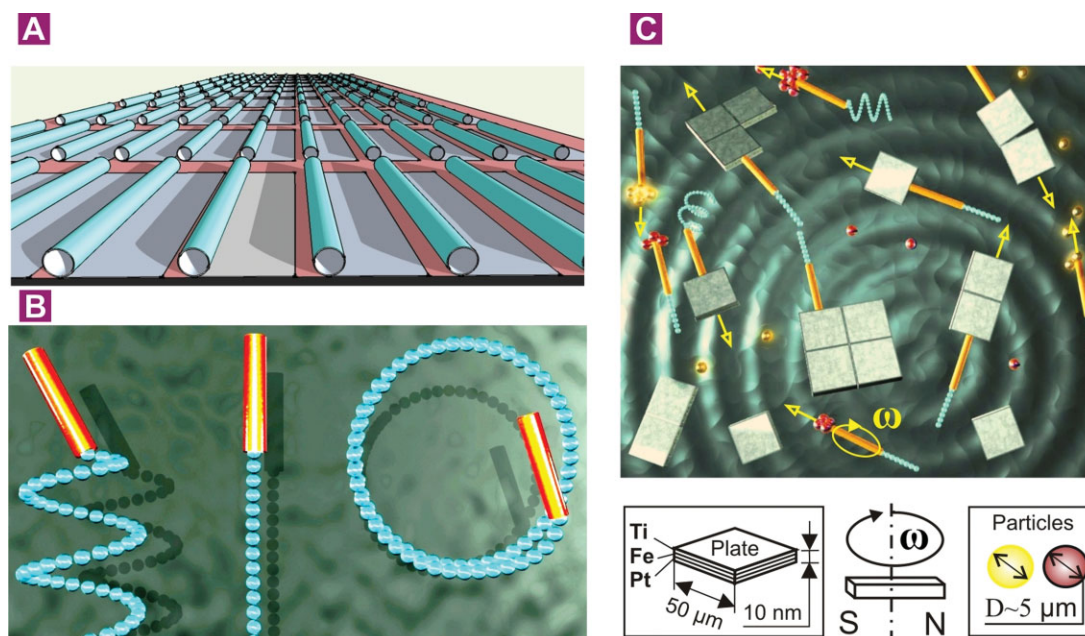

Figure 1. Schematic diagrams of: A) an array of rolled-up tubes, B) different autonomous trajectories of catalytic microtubes in H_2O_2 solution, and C) microfactory showing wireless control of microbots by an external magnet, assisted loading, transporting, delivery, and assembly of microparticles and nanoplates in fuel solution.

synchronize the magnetic field with the movement of the tubes. Therefore, if a straight motion of the microbots was desired, the magnet was left stationary. In contrast, by rotating the magnet, and thus changing the direction of the magnetic field, the microbots aligned themselves with the magnetic field. Being able to remotely control these microbots is an essential requirement for specialized and sophisticated tasks such as "wireless transport and delivery" of microscale loads and building blocks in a fluid. Figure 1C envisions the concept of a microfactory, where micro-objects are mixed together with synthetic microbots in a fluid and fuel is added in order to power them.

2.2. Bubble Propulsion Mechanism

The motion of our microbots is determined by bubble dynamics, similar to the catalytic millimeter-scale machines of Whitesides,[10] the bimetallic rod-based nanorotors of Ozin,[12] and the spherical microparticle-based motors of Gibbs and Zhao.[29] Rolled-up metallic tubes cannot be filled with water or hydrogen peroxide solutions because of their hydrophobic nature. Therefore, the addition of a surfactant (benzalkonium chloride used here) was required to mediate the capillary fluid filling, stabilize the bubbles, and reduce the surface tension.[30] Furthermore, the continuous generation of bubbles and their aggregation on the interface interfered with the visualization of the microbots. The addition of isopropanol (surface tension $= 21.7\,mJ\,m^{-2}$) was necessary to dramatically reduce the local high surface tension of the peroxide solution (surface tension (for 10 wt %) $= 73\,mJ\,m^{-2}$) and decrease the bubble lifetime.[31] Thus, recording the motion of the microbots was facilitated in this way as the vast majority of bubbles dissipated immediately after the addition of $10\,\mu L$ isopropanol to 1 mL of the fuel solution. We studied how hydrogen peroxide and the surfactant concentration affect the speed of the microtubes. The inset in Figure 2 represents the average microbot speeds as a function of surfactant concentration (5×10^{-5}, 20%) using a constant concentration of 15 wt % of H_2O_2. Each data point was taken as an average speed of five moving microbots. The experimental results reveal that a surfactant concentration beyond a certain threshold is required to activate the motion of the microbots. However, the speed of the microbots was reduced by further increasing the surfactant concentration. It is well known that the surface tension decreases strongly with increasing surfactant concentration. Above a certain concentration (critical micelle concentration, cmc) the surface tension becomes constant.[32] Moreover, the surfactant spontaneously forms aggregates (micelles) that can occupy the chemically active sites of the Pt catalyst film and, therefore, the observed speed is reduced beyond this concentration. A concentration of 0.005 wt % of surfactant was selected as the optimum for further experiments as it reduced the surface tension without inhibiting the chemical catalytic reaction. Figure 2 depicts the speed of the microtubes at different fuel (hydrogen peroxide) concentrations using a constant concentration of 0.005 wt % of the benzalkonium chloride surfactant. The speed increased with hydrogen peroxide concentration up to 15%, reaching a maximum speed of $275\,\mu m\,s^{-1}$ (5.5 body lengths per second), and it leveled off at higher concentrations. We note that the inner tube wall and surfactant choice was not optimized for speed as we did in our previous
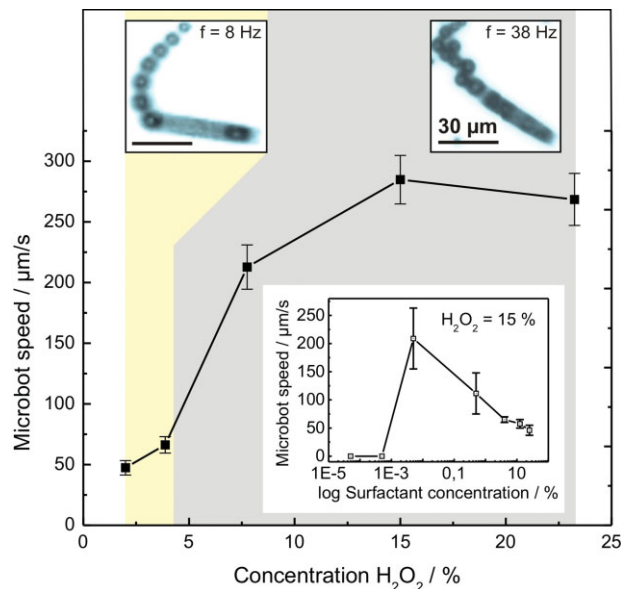

Figure 2. Speed of microtubes with different concentrations of hydrogen peroxide containing constant amount of surfactant (0.005 wt % benzalkonium chloride) and 1 vol % of isopropanol. The inset shows the speed of the microtubes with different concentrations of surfactant (5×10^{-5} to 20%) at 15 wt % of H_2O_2.

publication.[15] The plot shows similar features to a traditional Langmuir adsorption isotherm, which relates the adsorption of molecules on a solid surface to the concentration of the medium.[33] We hypothesize that the maximum speed is limited by i) the surface area of the Pt catalyst layer and ii) the intrinsic turnover rate of the catalyst at high analyte concentrations. For previously reported catalytic synthetic nanomotors their maximum speed was reached at different concentrations of H_2O_2: the bimetallic nanorods fabricated by Sen reached a maximum speed at 3.7 wt % of H_2O_2,[11] Wang reported similar results using carbon nanotubes (CNTs)- modified nanomotors but their highest speed was reached at 15 wt % of H_2O_2,[17] and Gibbs and Zhao observed maximum speeds of their microsphere-based motors at 2 wt % of H_2O_2.[29] In addition, we observed that there is a limited amount of space inside the microcavity at a high frequency of bubble generation ($f = 38\,Hz$), that is at high peroxide concentrations. The optical images in Figure 2 (inset) reveal that a microbot's speed is at its maximum when the maximum number of bubbles obtainable inside the cavity is generated. At lower peroxide concentrations, the frequency of bubble generation is lower ($f = 8\,Hz$), resulting in a lower speed of the microbots. This observation supports our quantitative study of the speed of microbots with respect to the fuel composition. Furthermore, it is in agreement with previously reported results, where the bubble frequency increases with increasing peroxide concentration.[15]

Figure 3 (i to iv) shows optical microscope images of the nucleation, growth, and migration mechanism of bubbles inside the microtubes within a time interval of 100 ms. The schematic insets of Figure 3 depict how the fluid is i) drawn into the tube, ii) a bubble nucleates upon the decomposition of H_2O_2 induced by the catalytic surface of platinum, iii) the O_2 bubble starts to grow and moves to the larger tube opening indicated by the black arrow, and
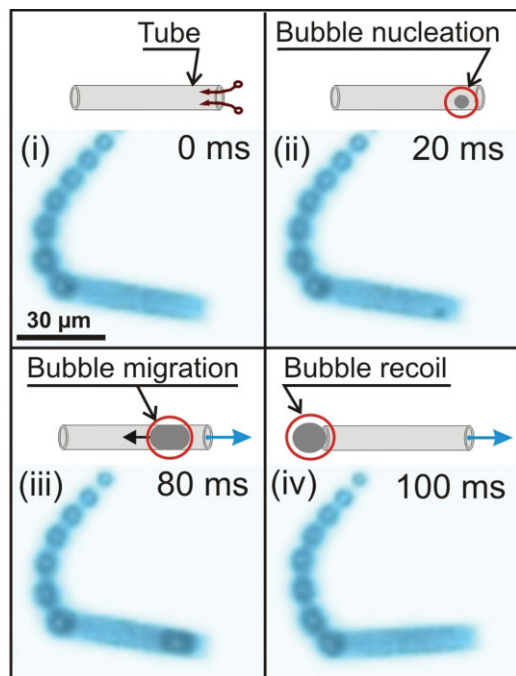
Figure 3. Bubble-propulsion mechanism: i) solution fills the tube. ii) The Pt catalytic surface induces the decomposition of H_2O_2 fuel and the generation of an O_2 bubble. iii) Bubble growth and movement to the opposite site producing a migration step of the tube. iv) The bubble is released thrusting the tube as it leaves, providing a recoil step. The direction of the tube motion is shown by blue arrow bars. (See also video #2, SI).

iv) the bubble recoils from the tube. Both bubble migration (iii) and recoil (iv) induce fluid pumping, which propels the tube into the opposite direction (blue arrow) (see also Video #2, SI).

2.3. Easy Loading and Moving of Particles

The suction of fluid into the tubular microbots induces an inward fluid motion that streamlines near the entrance of the tubes, dominating over the Brownian diffusion of the particles to be loaded. Therefore, when these particles are located close enough to the microbots, they remain adsorbed at the entrance of the tubes. Once the particles are positioned at the entrance of the tube, the suction is inhibited, which allows a Brownian diffusion of the particles away from the tube so that the particles are no longer tightly adsorbed. This movement, in turn allows more fuel to enter the tube and the pumping to restart. This process is repeated in a cyclic manner as seen in Video #3 in the Supporting Information.

Our system was able to selectively load a large number of particles. For a controlled loading and delivery of microparticles, we placed a magnet close to the microbot suspension containing the fuel solution and

microparticles as shown in Figure 1C. Suspended polystyrene microparticles (5 μm in diameter) were dispersed in a fluid and moved by Brownian diffusion. We slowly moved the poles of the magnet into the desired direction for the microbots to perform a specific task (the rotation of the magnet was slower than 1 rev s^{-1}). For example, one of the moving microbots was turned until its axis directly pointed to the particles; the trajectory was then kept in a straight line to pick up the particles. Finally, we turned the magnet (and the tube) at an angular speed larger than one revolution per second to deliver the particles.

Figure 4A shows a sequence of optical microscope images a of microbot transporting i) 3, ii) 27, iii) 44, and iv) 58 polystyrene particles (see also Video #4, SI). Figure 4B presents a quantitative study of the microbot speed as a function of the number of loaded particles in 5% peroxide solution. We used a low concentration of peroxide solution here as the fuel for observational convenience. As expected, a decrease of the speed from 80 to 18 μm·s^{-1} occurred because of the increased drag force when a larger number of microparticles were adsorbed. The drag force of a single microparticle depends linearly on its velocity at low Reynolds numbers and can be calculated using the Stokes drag formula

$$F_{drag} = 6\pi\eta r\upsilon \tag{1}$$

where υ is the particle velocity, η the fluid viscosity, and r the radius of the particle. The Stokes drag force for one particle moving at a velocity of 80 μm·s^{-1} is calculated to be 3.77 pN, and we achieved to transport up to 60 particles. It is remarkable that the microbot loaded with such a large number of particles can overcome the diffusion of the microparticles and the large drag force. Even more importantly, no chemical modification or functional attachments were needed during
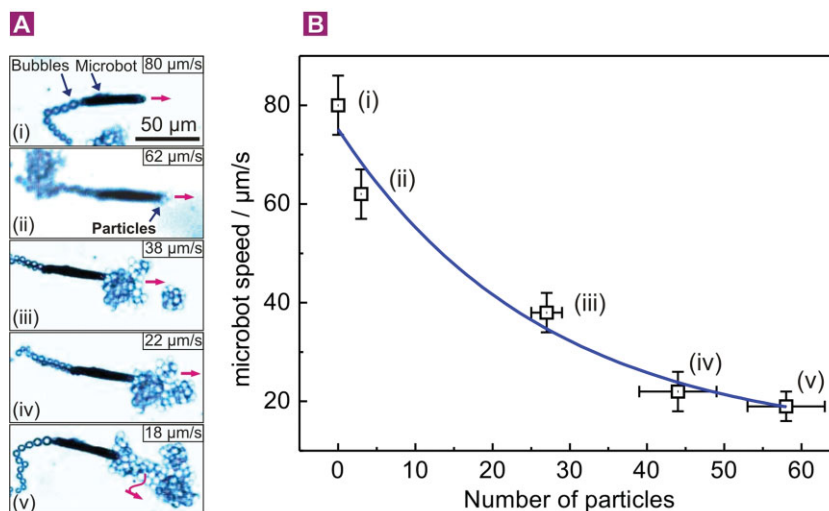

Figure 4. Transport of polystyrene microparticles of 5 μm diameter: A) Optical microscope images of a microbot loading and transporting ii) 3, iii) 27, i) 44, and iv) 58 particles. The insets show the average speed of the microbot. B) Plot depicting the speed of the microbots depending on the number of loaded microparticles. (See also video #4, SI). The red arrow bar shows the direction of particle motion assisted by the microbot. The fuel solution used: hydrogen peroxide (5 wt %), 0.005% surfactant, and 1 vol % isopropanol.

delivery since the pumping mechanism alone is responsible for loading and unloading. Finally, we observed that the precise control of the microbots using a magnetic field was not affected by the size of the cargo (see Video #4, SI). This led us to believe that the transport of a wide variety of cargo should be possible.

One example that verifies this hypothesis is the achievement of the directed transportation, assembly, and reorganization of Ti/Fe/Pt nanoplates (25 nm thick and 50 μm wide) on a liquid surface. The plot in Figure 5A shows self-propelled microbots transporting 1 to 4 nanoplates (i–v) in a 5% hydrogen peroxide solution (see also Video #5, SI).The thin Ti/Fe/Pt plates were anchored at the fluid/air interface because of their hydrophobic nature. The microbots were filled with oxygen gas, which also moves them to the fluid/air interface (schematically shown in the inset of Fig. 5A) because of the buoyancy force. The nanoplates contained ferromagnetic (Fe) layers for easy alignment towards the moving microbots, so that the magnetic field caused the rotation but not a linear displacement of the nanoplates. Once one nanoplate was transported, we directed the microbot to other nanoplates until the loading of four consecutive objects was achieved. An inverse exponential behavior of the speed was observed as the surface area of the transported plates increased. Figure 5B shows optical images of the microbot loading, transporting, and assembly of the nanoplates, which correspond to the experimental points (i–v) in Figure 5A.

Different assembly configurations of the nanoplates could be accomplished by wireless control of the microbot delivery as shown in Figure 6 (a–f). After loading 3 consecutive objects (Fig. 6c), we turned the magnetic field so that the nanoplates could change configuration (Fig. 6d), for example Figure 6f shows four nanoplates assuming a square shape. A video clip showing the loading of nanoplates in different configurations can be found in the Supporting Information (Video #6).
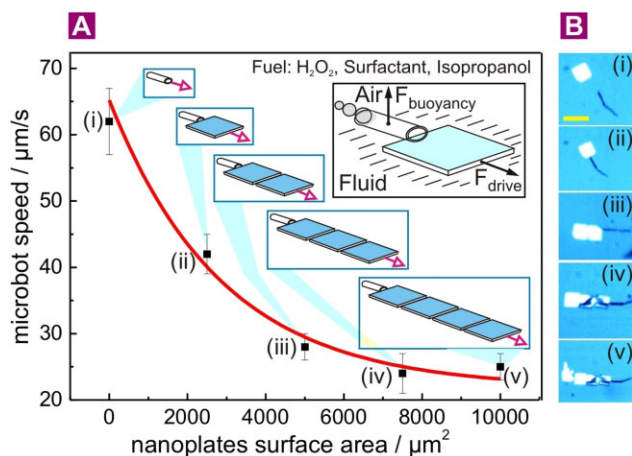

Figure 6. Optical images of a microbot assembling four nanoplates in different configurations (a–f) (See also video #6, SI). Fuel solution used: hydrogen peroxide (5 wt %), 0.005% surfactant, and 1 vol % isopropanol.

3. Conclusions

We have demonstrated the directed loading and transport of micro-objects by high propulsion powered rolled-up microbots (Ti/Fe/Pt) driven by a microbubble propulsion mechanism. The loading of particles was facilitated by the pumping of fluid into the microtubes via a catalytic reaction. The ferromagnetic (Fe) thin films introduced into the microtubes assisted the wireless motion directed by an external magnetic field. The extraordinarily easy control over the movement of the microbots by changing the direction of the magnetic field during motion helped to accurately load and deliver cargo at desired places. Our microbots had enough power to carry great numbers of particles or even large particles without any modification. We demonstrated that tubular microbots can load and delivery different kinds of materials, namely, both polymeric and metallic particles. The presented results are encouraging to construct universal drug-delivery systems, however, biocompatible fuels such as glucose would then have to be used, and these systems need to be explored further.

4. Experimental

Preparation of Rolled-up Microtubes: Ti/Fe/Pt microtubes were fabricated by electron-beam (e-beam) evaporation (Ti/Fe) and magnetron sputtering (Pt) of thin metallic films on patterned photoresist squares with a single element size of 50 μm × 50 μm. Photoresist AR-P 3510 was spin-coated on silicon wafers (1.5 inch) at 3500 rpm for 35 s, followed by a soft bake using a hotplate at 90 °C for 1 min and exposure to UV light with a Karl Suss MA-56 mask aligner (410–605 nm). Photoresist patterns were then developed in an AR300-35/H_2O solution (1:1). Rolled-up catalytic microtubes were obtained by a tilted deposition at an angle of about 60° (measured from the horizontal axis) on the photoresist. Metallic particle films (Ti/Fe) with thicknesses of 10 nm (Ti) and 5 nm (Fe) were deposited layer by layer on the tilted samples. Then, by using magnetron sputtering, 2 nm of Pt were deposited onto the Ti/Fe samples. The samples were immersed in acetone where rolling-up of the thin metallic films into microtubes was achieved by selectively etching the photoresist layer. Supercritical point drying was used in order to avoid collapsing of the tubes because of high fluid surface tension. For catalytic motions the microtubes

Figure 5. Wireless selective assembly of metallic nanoplates mediated by microbots. A) Effect of number of transported nanoplates on the microbot speed. The insets show schematic diagrams of the microbot moving one nanoplate (upper image). B) Optical images of the microbot corresponding to experimental points (i–v) in (A). (See also video # 5, SI). The error bar = 100 μm. The fuel solution used: hydrogen peroxide (5 wt %), 0.005% surfactant, and 1 vol % isopropanol.
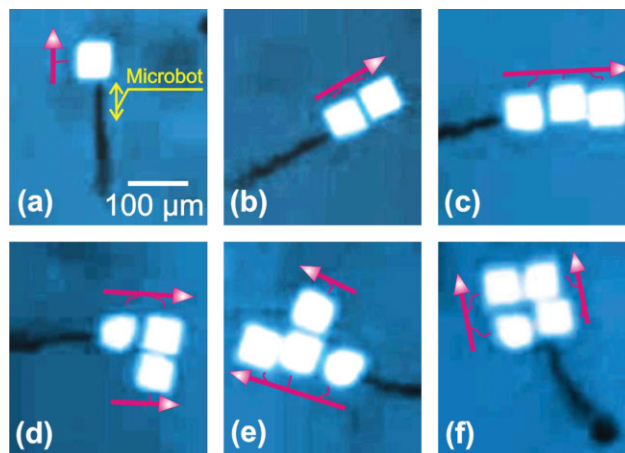
were usually gently released by mechanical scratching of the substrates in a fluid.

Microbots Motion: In order to investigate the speed of the microbots, various concentrations of hydrogen peroxide (1–25 wt %) at constant surfactant concentrations (0.005 wt % benzalkonium chloride, from Fluka Chemika) were prepared. The effect of the surfactant was studied by mixing a hydrogen peroxide solution at constant concentration (30 wt %) with solutions at different concentrations of benzalkonium chloride (5×10^{-5} to 20 wt %) in a 1:1 ratio. In order to locally reduce the fluid surface tension, a small amount (1%, v/v) of isopropanol was added.

Micro-objects Used as Cargo: Polystyrene microspheres (Duke Scientific Corp., 1% solids) with diameters of 1 μm and 5 μm were used in the experiments for particle transportation. Ti/Fe/Pt nanoplates were prepared in a similar way (Ti/Fe = 10:5 nm) as the microtubes described above, with a Pt thickness of 10 nm. This thickness covered all photoresist patterns (here, no shadow effect was used as in the case of the angular e-beam deposition). The patterns were then immersed in acetone, followed by rinsing in isopropanol, and placing the samples in hydrogen peroxide solution containing the self-propelled microtubes.

Optical Characterization of Motion: Optical microscope images were captured by a Zeiss Axiocam MRc camera and videos were recorded by using a high-speed camera (Photonic Science Limited) at 50 or 200 frames per second.

Acknowledgements

[1] a) G. A. Ozin, I. Manners, S. Fournier-Bidoz, A. Arsenault, *Adv. Mater.* **2005**, *17*, 3011. b) J. Wang, *ACS Nano* **2009**, *3*, 4. c) S. Sanchez, M. Pumera, *Chem. Asian J.* **2009**, *4*, 1402.

[2] R. P. Feynman, *Eng. Sci.* **1960**, *23*, 22.

[3] a) W. R. Browne, B. L. Feringa, *Nat. Nanotechnol.* **2006**, *1*, 25. b) M. Schliwa, G. Woehlke, *Nature* **2003**, *422*, 759.

[4] a) H. Yin, M. D. Wang, K. Svoboda, R. Landick, S. M. Block, J. Gelles, *Science* **1995**, *270*, 1653. b) M. V. Rodnina, M. Beringer, W. Wintermeyer, *Trends Biochem. Sci.* **2006**, *32*, 20.

[5] D. Stock, A. G. W. Leslie, J. W. Walker, *Science* **1999**, *286*, 1700.

[6] H. C. Berg, *Annu. Rev. Biochem.* **2003**, *72*, 19.

[7] R. B. Vallee, P. A. Hook, *Nature* **2003**, *421*, 701.

[8] K. Svoboda, C. F. Schmidt, B. J. Schnapp, S. M. Block, *Nature* **1993**, *365*, 721.

[9] K. Kinbara, T. Aida, *Chem. Rev.* **2005**, *105*, 1377.

[10] R. F. Ismagilov, A. Schwartz, N. Bowden, G. M. Whitesides, *Angew. Chem. Int. Ed.* **2002**, *41*, 652.

[11] W. F. Paxton, K. C. Kistler, C. C. Olmeda, A. Sen, S. K. St. Angelo, Y. Cao, T. E. Mallouk, P. E. Lammert, V. H. Crespi, *J. Am. Chem. Soc.* **2004**, *126*, 13424.

[12] S. Fournier-Bidoz, A. C. Arsenault, I. Manners, G. A. Ozin, *Chem. Commun.* **2005**, 441.

[13] L. Qin, M. J. Banholzer, X. Xu, L. Huang, C. A. Mirkin, *J. Am. Chem. Soc.* **2007**, *129*, 14870.

[14] Y. F. Mei, G. S. Huang, A. A. Solovev, E. Bermudez Urena, I. Monch, F. Ding, T. Reindl, R. K. Y. Fu, P. K. Chu, O. G. Schmidt, *Adv. Mater.* **2008**, *20*, 4085.

[15] A. A. Solovev, Y. F. Mei, E. Bermudez Urena, G. Huang, O. G. Schmidt, *Small* **2009**, *5*, 1688.

[16] W. F. Paxton, A. Sen, T. E. Mallouk, *Chem. Eur. J.* **2005**, *11*, 6462.

[17] R. Laocharoensuk, J. Burdick, J. Wang, *ACS Nano* **2008**, *2*, 1069.

[18] U. K. Demirok, R. Laocharoensuk, K. M. Manesh, J. Wang, *Angew. Chem. Int. Ed.* **2008**, *47*, 9349.

[19] N. S. Zacharia, Z. S. Sadeq, G. A. Ozin, *Chem. Commun.* **2009**, 5856.

[20] a) T. R. Kline, W. F. Paxton, T. E. Mallouk, A. Sen, *Angew. Chem. Int. Ed.* **2005**, *44*, 744. b) P. Calvo-Marzal, K. M. Manesh, D. Kagan, S. Balasubramanian, M. Cardona, G.-U. Flechsig, J. Posner, J. Wang, *Chem. Commun.* **2009**, 4509. c) S. Balasubramanian, D. Kagan, K. M. Manesh, P. Calvo-Marzal, G.-U. Flechsig, J. Wang, *Small* **2009**, *5*, 1569. d) M. Ibele, T. E. Mallouk, A. Sen, *Angew. Chem. Int. Ed.* **2009**, *48*, 3308.

[21] J. Burdick, R. Laocharoensuk, P. M. Wheat, J. D. Posner, J. Wang, *J. Am. Chem. Soc.* **2008**, *130*, 8164.

[22] S. Sundararajan, P. E. Lammert, A. W. Zudans, V. H. Crespi, A. Sen, *Nano Lett.* **2008**, *8*, 1271.

[23] O. G. Schmidt, K. Eberl, *Nature* **2001**, *410*, 168.

[24] W. F. Paxton, P. T. Baker, T. R. Kline, Y. Wang, T. E. Mallouk, A. Sen, *J. Am. Chem. Soc.* **2006**, *128*, 14881.

[25] H. A. Stone, A. M. Forsyth, J. Wan, *Physics* **2009**, *2*, 89.

[26] a) R. Dreyfus, J. Baudry, M. L. Roper, M. Fermigier, H. A. Stone, J. Bibette, *Nature* **2005**, *437*, 862; b) S. C. Schuster, S. Khan, *Annu. Rev. Biophys. Biomol. Struct.* **1994**, *23*, 509.

[27] S. C. Kuo, J. L. McGrath, *Nature* **2000**, *407*, 1026.

[28] C. Wohlgemuth, E. Hoiczyk, D. Kaiser, G. Oster, *Curr. Biol.* **2002**, *12*, 369.

[29] J. G. Gibbs, Y.-P. Zhao, *Appl. Phys. Lett.* **2009**, *94*, 163104.

[30] R. Mohammadi, J. Wassink, A. Amirfazli, *Langmuir* **2004**, *20*, 9657.

[31] G. Londe, A. Chunder, A. Wesser, L. Zhai, H. J. Cho, *Sens. Actuators B* **2008**, *132*, 431.

[32] H.-J. Butt, K. Graf, M. Kappl, in: *Physics and Chemistry of Interfaces*, Wiley-VCH, Weinheim, Germany **2003**, Ch. 9 and 12.

[33] W. Stumm, (Ed.), in *Chemistry on the Solid-Water Interface*, John Wiley and Sons, New York, NJ **1993**, Ch. 4.